

Modelling pH-Dependent and Microstructure-Dependent Streaming Potential Coefficient and Zeta Potential of Porous Sandstones

P. W. J. Glover¹

Received: 30 November 2017 / Accepted: 7 March 2018 / Published online: 17 May 2018
© The Author(s) 2018

Abstract In this paper, we have significantly modified an existing model for calculating the zeta potential and streaming potential coefficient of porous media and tested it with a large, recently published, high-quality experimental dataset. The newly modified model does not require the imposition of a zeta potential offset but derives its high salinity zeta potential behaviour from Stern plane saturation considerations. The newly modified model has been implemented as a function of temperature, salinity, pH, and rock microstructure both for facies-specific aggregations of the new data and for individual samples. Since the experimental data include measurements on samples of both detrital and authigenic overgrowth sandstones, it was possible to model and test the effect of widely varying microstructural properties while keeping lithology constant. The results show that the theoretical model represents the experimental data very well when applied to model data for a particular lithofacies over the whole salinity, from 10^{-5} to 6.3 mol/dm^3 , and extremely well when modelling individual samples and taking individual sample microstructure into account. The new model reproduces and explains the extreme sensitivity of zeta and streaming potential coefficient to pore fluid pH. The low salinity control of streaming potential coefficient by rock microstructure is described well by the modified model. The model also behaves at high salinities, showing that the constant zeta potential observed at high salinities arises from the development of a maximum charge density in the diffuse layer as it is compressed to the thickness of one hydrated metal ion.

Keywords Microstructure · Porosity · Streaming potential · Zeta potential · Electrical rock properties

✉ P. W. J. Glover
p.w.j.glover@leeds.ac.uk

¹ School of Earth and Environment, University of Leeds, Leeds LS2 9JT, UK

List of Symbols

C_f	Pore fluid salinity (mol/dm ³)
C_{sp}	Streaming potential (coupling) coefficient with respect to pressure (mV/MPa)
F	Formation factor, $F = \phi^{-m}$ (-)
K_1	Equilibrium constant for solution of CO ₂ in water. $pK_1 = -\log_{10} K_1$ (-)
K_2	Equilibrium constant for solution of CO ₂ in water. $pK_2 = -\log_{10} K_2$ (-)
$K_{(-)}$	Disassociation constant for dehydrogenization of silanol surface sites. $pK_{(-)} = -\log_{10} K_{(-)}$ (-)
K_{me}	Binding constant for cation adsorption. $pK_{me} = -\log_{10} K_{me}$ (-)
K_w	Disassociation constant of water. $pK_w = -\log_{10} K_w$ (-)
N	Avogadro's number, $\sim 6.022 \times 10^{+23}$ /mol (mol ⁻¹)
pH_{expt}	pH at which the experiments were run (arithmetic mean value) (-)
$pH_{st.dev}$	Standard deviation in pH_{expt} (-)
T	Temperature (°C or K)
a	1. Fitting parameter in Eq. (1) for zeta potential (mV). 2. Constant in the Theta Transformation, $= 8/3$ for clastic rocks (-)
b	Fitting parameter in Eq. (1) for zeta potential (mV)
d_{gr}	Modal grain diameter (m)
e	Elementary charge, $\sim 1.602 \times 10^{-19}$ C (C)
k	Boltzmann's constant, $\sim 1.3806 \times 10^{-23}$ J/K (J/K)
m	Cementation exponent (-)
β_{Na^+}	Na ⁺ Ionic fluid mobility (m ² /s/V)
β_{H^+}	H ⁺ Ionic fluid mobility (m ² /s/V)
β_{Cl^-}	Cl ⁻ Ionic fluid mobility (m ² /s/V)
β_{OH^-}	OH ⁻ Ionic fluid mobility (m ² /s/V)
β_{Stern}	Stern layer mobility
ϵ_r	Relative dielectric permittivity of the pore fluid (-)
ϵ_0	Absolute dielectric permittivity of a vacuum, $\sim 8.854 \times 10^{-12}$ F/m (F/m)
ζ	Zeta potential (mV)
η_f	Pore fluid viscosity (Pa s)
σ_s	Measured surface conductivity (-)
ϕ	Total porosity (-)
$\chi\zeta$	Shear plane distance (m)
Γ_s^0	Density of mineral surface sites for complexation (sites/nm ²)
Λ	Characteristic length scale of the pores (m)
Σ_s^{Prot}	Protonic surface conductance/specific conductivity (S)
Σ_s	Total surface conductance/specific conductivity (S)

1 Introduction

The only existing theoretical model for the streaming potential coefficient (C_{sp}) and zeta potential (ζ) in porous media was proposed by Glover et al. (2012) and introduced a parameter called the zeta potential offset. However, the data on which it was tested were not of sufficient quality to allow validate it fully, especially as a function of pH and rock microstructure. There also remained the difficulty of interpreting the physical meaning of the zeta potential offset parameter. This empirical parameter was included in the Glover et al. (2015) model because

its inclusion allowed the model to work well. However, at the time of its inclusion it had no satisfactory formal interpretation.

Consequently, an experimental campaign was initiated to produce a large database of 1253 measurements of C_{sp} and ζ of the highest possible quality, using pore fluids which were fully equilibrated with the rock samples, where pore fluid salinity, conductivity and pH were all accurately measured, which were supported by a full suite of associated petrophysical measurements made on individual samples, and where the dataset contains a large number (324) of measurements with a salinity $C_f > 1 \text{ mol/dm}^3$ (Walker and Glover 2017). The availability of this dataset offers the opportunity to carry out a detailed modelling campaign.

This paper reports that modelling campaign, and is, we believe, the most comprehensive modelling of C_{sp} and ζ carried out so far. The first aim of the work described in this paper was to modify the existing C_{sp} and ζ theoretical model (Glover and Déry 2010; Glover et al. 2012, 2015) in order to fully represent pH variation in electrolytes. In previous models, the pH was allowed to vary as a function of temperature and with the addition of acids and bases but not as a function of salinity. The second aim was to replace the unjustified zeta potential offset with a modelling approach that takes into account the development of a maximum charge density in the diffuse layer as it is compressed to the thickness of one hydrated metal ion in thickness at high salinities. The third aim was to attempt to model the data of Walker and Glover (2017) both by facies and for individual rock samples and, in so doing, confirm (1) the operation of the low salinity control of microstructure on C_{sp} , (2) examine the role of pH variations on C_{sp} and ζ , and (3) investigate the possible physical causes of the zeta potential offset hypothesized by Jaafar et al. (2009) and Vinogradov et al. (2010).

There have been several attempts to model the ζ and C_{sp} of rocks. Pride and Morgan (1991) produced an empirical fit to 35 existing ζ data as a function of salinity in the low salinity range, $C_f < 0.1 \text{ mol/dm}^3$. They obtained

$$\zeta = a + b \log_{10}(C_f), \quad (1)$$

where ζ is in volts and C_f is in mol/dm^3 , $a = +8 \text{ mV}$ and $b = +26 \text{ mV}$. Although this relationship describes the main aspects of the data to which it was fitted well, it provides positive ζ at salinities $> 0.5 \text{ mol/dm}^3$, whereas the physical model of the mineral/fluid interface would predict a negative value trending towards zero, and all measurements that have been made so far at high salinities provide extremely small but negative values (Jaafar et al. 2009; Vinogradov et al. 2010; Walker et al. 2014, Walker and Glover 2017). Similar empirical fits have been carried out by a number of authors with similar results: Walker and Glover (2017) provided $a = +3.505 \pm 28.823 \text{ mV}$ and $b = +11.33 \pm 4.06 \text{ mV}$ and for their entire dataset as well as carrying out fits to individual facies, Vinogradov et al. (2010) obtained $a = +9.67 \text{ mV}$ and $b = +19.02 \text{ mV}$, Jaafar et al. (2009), which share some data with Vinogradov et al. (2010), suggested $a = +6.43 \text{ mV}$ and $b = +20.85 \text{ mV}$. Bolève et al. (2007) suggested $a = +14.6 \text{ mV}$ and $b = +29.1 \text{ mV}$, while Revil et al. (1999a) have estimated the values at $a \approx +10 \text{ mV}$ and $b \approx +20 \text{ mV}$. However, these fits are simply empirical relationships. Their similarity (as shown in Fig. 1) underlines a general trend. However, all of these fits produce positive ζ at high salinities, whereas none of the 400 or so measurements for $C_f > 1 \text{ mol/dm}^3$ so far are positive (Jaafar et al. 2009; Vinogradov et al. 2010; Walker and Glover 2017); they all have small constant negative values instead. Clearly the empirical approach is limited, and a physically based theoretical model is required.

In the late 1990s, a series of papers allowed a theoretical model for ζ to be constructed (Revil and Glover 1997, 1998; Revil et al. 1999a). Equation (1) is obtained theoretically in the last of these papers. Revil et al. (1999a) applied a number of simplifying assumptions to

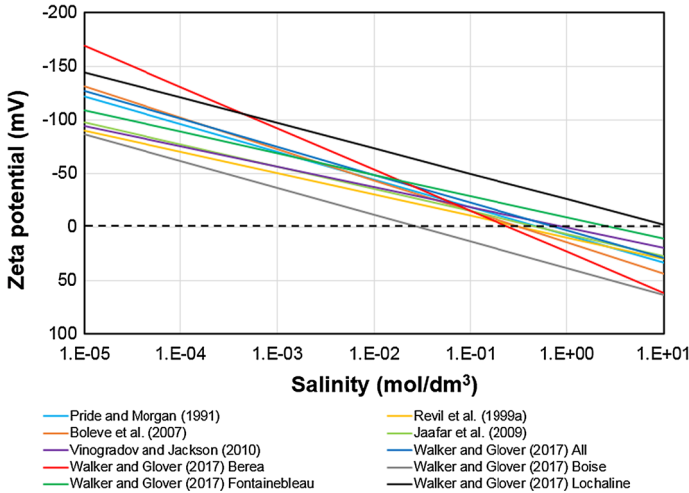


Fig. 1 Representation of 10 existing empirical fits of ζ as a function of pore fluid salinity showing approximately the same behaviour but with unexplained high salinity behaviour and variability with pH

their more general equations, which were (1) that $\text{pH}=7$, (2) that the fluid is an Na^+ or K^+ symmetric electrolyte, (3) that the influence of H^+ and OH^- ions on the ionic strength of the solution saturating the pores can be neglected (Revil and Glover 1997), and (4) that direct adsorption of K^+ and Na^+ ions upon the silica surface can also be neglected.

Under these conditions

$$a = \frac{2kT}{3e} \ln \left\{ \frac{\sqrt{8000 \epsilon_r \epsilon_0 k T N}}{2e \Gamma_s^\circ K_{(-)}} 10^{-\text{pH}} \right\}, \tag{2}$$

and

$$b = \frac{kT}{3e} \log_e 10, \tag{3}$$

where k is Boltzmann’s constant ($\sim 1.3806 \times 10^{-23}$ J/K), T is the temperature (in K), e is the elementary charge ($\sim 1.602 \times 10^{-19}$ C), ϵ_r is the relative dielectric permittivity of the pore fluid, ϵ_0 is the absolute dielectric permittivity of a vacuum ($\sim 8.854 \times 10^{-12}$ F/m), N is Avogadro’s number ($\sim 6.022 \times 10^{23}$ /mol), Γ_s° is the density of surface sites, and $K_{(-)}$ is the disassociation constant for dehydrogenization of silanol surface sites. The gradient of ζ versus $\log_{10}(C_f)$ then depends only on temperature with $b=+19.38$ mV when $T=20^\circ\text{C}$, while the offset at the same temperature is $a = +16.89$ mV for reasonable choices of its input parameters ($\text{pH} \equiv 7$, $\Gamma_s^\circ = 10$ sites/ nm^2 , $K_{(-)} = 10^{-8}$, and assuming $\epsilon_r = 80$), which are discussed later in this paper. This model gives values of ζ which remain negative for the entire salinity range, tending towards zero at high salinities ($C_f \approx 7.4$ mol/ dm^3 , which is just higher than the saturation limit for NaCl in water at $C_{\text{sat}} \approx 6.16$ mol/ dm^3) as required by the physical model.

Although the ζ could be calculated from the Revil et al. (1999a) model without the restrictions used to produce Eqs. (2) and (3), or from a more complex calculation that accounts for a variable pH, calculation of C_{sp} remained more difficult. One approach would be to use the classical Helmholtz–Smoluchowski (H–S) equation (e.g., Glover et al. 2015; Walker and Glover 2017), but as the H–S equation has only been validated for capillary tubes, the

result would not take into account the properties of the rock such as porosity, grain size and cementation exponent. In 2010, Glover and Déry (2010) provided the equations required to calculate the C_{sp} of individual rocks, taking into account their individual microstructural properties. That paper, which considered packs of glass beads, implemented a full theoretical description of ζ (Revil et al. 1999a), and C_{sp} was then calculated for the grain size, porosity and cementation exponent of the glass bead packs. The modelling was capable of representing the sigmoidally shaped variation of streaming potential with grain size (Glover and Déry 2010), but was restricted to the ideal matrix geometry imposed by the bead packs.

The theory was developed further and published in a form which could be applied to porous granular media (Glover et al. 2012) and was validated against a database of 290 C_{sp} and 269 ζ measurements made by a large number of researchers. Unfortunately this database did not contain sufficient information about the salinity, electrical conductivity and pH of the fluids in contact with the grains of the rock at the time that the streaming potential measurement was made. In many cases, the experimental temperature was not measured or reported and information about the microstructural properties of the samples that were being measured was not measured or given. Although this dataset represented all the data that were available, it was not considered a stringent test of the theoretical model. Consequently, new experimental approaches (Walker et al. 2014) were developed to make a large number of well-constrained measurements for testing the model, which are reported in full in Walker and Glover (2017) and form the experimental base with which the modelling in this paper is compared.

2 Reference Data

A full description of the reference data can be found in Walker and Glover (2017). This modelling uses the entire dataset of 1253 C_{sp} measurements and their derived ζ , representing 14 samples of 4 sandstone facies (Berea, Boise, Lochaline and Fontainebleau sandstones). Several separate examples of Fontainebleau and Lochaline sandstones composed of sub-rounded detrital grains, and consisting of detrital grains with euhedral quartz overgrowths, were measured (distinguished by the additional letter 'D' and 'Q' in the sample codes, respectively). A brief summary of sample properties measured during initial characterisation is shown in Table 1 of Walker and Glover (2017). The quality of the experimental data is generally good, having been measured at pore fluid equilibrium and with well-defined salinity and pH. However, the early data from one of the Berea sandstone (BR1) and one of the Boise sandstone samples (BIII) are less good and this is due to immature experimental protocols, as described in Walker and Glover (2017).

3 Electro-kinetic Modelling

The theoretical model used in this work is based on the electro-chemical approach to modelling the electrical double layer (Pride 1994; Revil and Glover 1997; 1998; Revil et al. 1999a; Glover et al. 2012). It has been modified for this paper by (1) the inclusion of a variable pH that is a function of temperature, added acid, added base, and salinity, (2) improvements to the calculation and temperature and salinity dependencies of the fluid properties, and (3) the implementation of implicit modelling of the high salinity ζ obviating any need for the zeta potential offset as in previous models (e.g., Glover et al. 2012).

Table 1 Model parameters

Parameter type	Parameters	Status and value	Sources
<i>Fixed parameters</i>			
Experimental conditions	Temperature T (°C and K)	Fixed: From experimental data	Walker and Glover (2017)
Fundamental physical constants	Permittivity in vacuo	Fixed: 8.850×10^{-12} F/m	Lide (2017)
	Boltzmann's constant	Fixed: 1.381×10^{-23} J/K	Lide (2017)
	Avagadro's constant	Fixed: $6.022 \times 10^{+23}$ /mol	Lide (2017)
	Electronic charge	Fixed: 1.602×10^{-19} C	Lide (2017)
Pore fluid parameters	Na ⁺ Ionic fluid mobility	Fixed: 5.20×10^{-8} m ² /s/V	Crow (1988)
	H ⁺ Ionic fluid mobility	Fixed: 3.63×10^{-7} m ² /s/V	Crow (1988)
	Cl ⁻ Ionic fluid mobility	Fixed: 7.90×10^{-8} m ² /s/V	Crow (1988)
	OH ⁻ Ionic fluid mobility	Fixed: 2.05×10^{-7} m ² /s/V	Crow (1988)
	Disassociation constant K_w	Fixed: 7.801×10^{-15} mol/dm ³	Calculated in the model using Lide (2017)
	Equilibrium constant pK_1 (-)	Fixed: 2.95121×10^{-8}	Wu et al. (1991) and Revil et al. (1999a, b)
	Equilibrium constant pK_2 (-)	Fixed: 5.01187×10^{-11}	Wu et al. (1991) and Revil et al. (1999a, b)
	Fixed mineral/pore fluid interface parameters	Stern layer ionic mobility β_{Stern}	Fixed: 5×10^{-9} m ² /s/V
Surface site density Γ_o		Fixed: 10 sites/nm ²	Revil and Glover (1998)
Cation adsorption binding constant pK_{Me}		Fixed: 7.5	Kosmulski (1996)
Shear plane distance $\chi\zeta$		Fixed: 2.4×10^{-9} m	Revil et al. (1999a, b)
Microstructural parameters	Protonic surface conduction Σ_{prot} (S)	Fixed: Calculated in the model	Calculated in the model
	Modal grain size, d_{gr} (m)	Fixed: From experimental data	Walker and Glover (2017)
	Porosity, ϕ (-)	Fixed: From experimental data	Walker and Glover (2017)
	Cementation exponent, m (-)	Fixed: From experimental data	Walker and Glover (2017)
	Formation factor, F (-)	Fixed: Calculated in the model	Calculated in the model
	Characteristic pore size, Λ (m)	Fixed: Calculated in the model	Calculated in the model
	<i>Variable parameters</i>	Pore fluid salinity (mol/dm ³)	Varied between 10^{-5} and 10 mol/dm ³
Pore fluid pH (-)		For fixed values: pH 6, 6.5, 7, 7.5, 8	
Silanol dehydrogenization constant pK (-)		Variable: between 7.3 and 8.1	Dove and Rimstidt (1994), Kosmulski (1996), Hienstra and van Riemsdijk (1990), Rustad et al. (1998)

It should be noted that modelling has been carried out at the temperature at which the individual data were measured, but instead of implementing one modelling curve for the experimental pH, a range of different models with different pHs have been implemented and shown as 5 modelling curves which divide the zeta potential–pore fluid salinity space and streaming potential–pore fluid salinity space. This approach has the advantage of informing the reader how the model behaves with both changes in pore fluid salinity and pH in one plot. The experimental data are then added to the plot following a trend which lies on or is parallel to a curve for one of the modelled pHs. Conformity of the model to the experimental data can then be judged by comparing the experimentally derived pH (provided in the data tables) with that indicated by how the experimental data fall on the network of modelled curves for different pHs. Despite there being many variables in the model, only one, $K_{(-)}$, was varied to improve the conformity of the model curves to the experimental data, and then only over a very restricted range supported by independent measurements for this parameter (please see Sect. 3.7).

3.1 Modelling Procedure

The modelling has the following steps:

1. Define the temperature, fluid salinity range and fluid pH over which the modelling is to take place.
2. Calculate the density of pure water in kg/m^3 at the modelling temperature T in ($^{\circ}\text{C}$) using

$$\rho_w = 1000 \frac{1 - (T+288.9414)}{508929.2 \times (T+68.12963)} (T - 3.9863)^2. \quad (4)$$

3. Calculate the density of the NaCl solution (in g/cm^3) at the given salinity (in mol/dm^3) and temperature using

$$\rho_f = 58.44 C_f + \frac{\rho_w}{1000} \left(1000 - \frac{58.44 C_f}{2.16} \right). \quad (5)$$

4. Calculate the molality of the NaCl solution (in mol/kg) at the given salinities (in mol/dm^3) and temperature using

$$c_f = \frac{C_f}{(\rho_f - (58.44 C_f / 1000))}. \quad (6)$$

5. Calculate the pore fluid electric permittivity using Olhoeft's empirical equation (Revil et al., 1999b)

$$\varepsilon_f = \varepsilon_o \varepsilon_r = \varepsilon_o (a_0 + a_1 T + a_2 T^2 + a_3 T^3 + c_1 C_f + c_2 C_f^2 + c_3 C_f^3), \quad (7)$$

where $a_0 = 295.68$, $a_1 = -1.2283/\text{K}$, $a_2 = -2.094 \times 10^{-3}/\text{K}^2$, $a_3 = -1.41 \times 10^{-6}/\text{K}^3$, $c_1 = -13.00 \text{ dm}^3/\text{mol}$, $c_2 = -1.065 (\text{dm}^3/\text{mol})^2$, $c_3 = -0.03006 (\text{dm}^3/\text{mol})^3$, the temperature is in Kelvin and is valid in the range 273–373 K, the salinity is in mol/dm^3 and the permittivity *in vacuo* $\varepsilon_o = 8.854 \times 10^{-12} \text{ F/m}$ (Lide 2017).

6. Calculate the pore fluid electrical conductivity σ_f using Sen and Goode's method (Sen and Goode 1992a, b).
7. Calculate the pore fluid viscosity η_f using Phillips et al.'s method (Phillips et al. 1978; Glover et al. 2012). This method requires the use of the pore fluid molality (Eq. (6)).

8. Calculate the ionic concentration of the pore fluid including contributions from acids and bases that are added to perturb the pH to give the pH to be modelled. This step uses the imposed salinity with the addition of the concentrations of hydrogen and/or base ions to arrive at the desired pH value. It is not sufficient to calculate these from the desired pH and pOH because the pore fluid is also in equilibrium with atmospheric carbon dioxide. Consequently, the pH depends on the concentrations of hydrogen and base ions according to a cubic law. We solve the cubic law automatically in our model using Cardano's method (Glover et al. 2012). This approach also requires knowledge of the disassociation constant for water K_w , for which an empirical equation is available in Lide (2017) and described in full in Glover et al. (2012).
9. Calculate the ζ of the sample (Glover et al. 2012).
10. Calculate the C_{sp} of the sample (Glover et al. 2012).

The model outputs for this work are C_{sp} and ζ . The calculation of C_{sp} requires three additional parameters, which are all microstructural parameters that are specific to the individual rock sample. The ζ is calculated for a given mineralogy, fluid type (electrolyte type, salinity and pH) and temperature and is usually considered to be independent of the microstructure of the individual rock, while it is clear from experiments that C_{sp} depends upon the microstructure of the individual rock, at least at low salinities (Glover et al. 2015; Walker and Glover 2017).

All parameters are discussed below, separating them into groups. The parameters used in this paper for the modelling by rock type and for individual samples can be found in Tables 2 and 3, respectively, together with a note of their sources. It should be noted that while many parameters contribute to the model, almost all are fixed either by independent experimental measurements made in this paper or by other researchers or perform as modelling variables.

3.2 Modelling Variables

There are three parameters which are modelling variables. These are temperature, salinity and pH. In this work, the salinity and pH have been varied between 10^{-5} and 10 mol/dm^3 , and between pH 5.5 and pH 8.5, respectively. The salinity is used to calculate the concentration of ions in the solution together with the concentration of H_3O^+ and OH^- , which are calculated from the fluid pH. The model is not strongly sensitive to temperature. Nevertheless, the temperature for each modelling run has been fixed to the mean experimental temperature given in Walker and Glover (2017).

3.3 Pore Fluid Parameters

There are six parameters which describe the pore fluid. Four describe the ionic mobilities. Since it was assumed that the electrolyte was a simple symmetric monovalent NaCl solution in this work, the four ionic mobilities are those for Na^+ , Cl^- , H^+ and OH^- (Crow 1988). The disassociation constant K_w is required in the model, but it is not an input parameter because we calculate it from the temperature using the empirical relationship of Lide (2017). The disassociation constant of water varies little in the range of temperatures encountered in the experimental data modelled by this work, which were from 20.1 to 27.2 °C, and takes values from $10^{-14.17}$ to $10^{-13.97}$, respectively. The two remaining input parameters are equilibrium constants which describe the reaction of the electrolyte with atmospheric carbon dioxide (Glover et al. 2012); fixed at $pK_1 = 7.53$ and $pK_2 = 10.3$ after Wu et al. (1991) and Revil et al. (1999a).

Table 2 The mean values of parameters used in the modelling of the ζ and C_{sp} for each rock type together with their source

Parameter	Units	Source	Berea sandstone	Boise sandstone	Detrital Fontainebleau sandstone F1D and F2D	Overgrown Fontainebleau sandstone F3Q and F4Q	Detrital Lochaline sandstone L1D and L2D	Overgrown Lochaline sandstone L3Q and L4Q
Samples			BR1, BR2 and BR3 (a)	B1II, B2II and B3I (b)	(c)	(d)	(e)	(f)
Part of Figs. 2 and 3								
<i>Fluid parameters</i>								
Fluid type			NaCl	NaCl	NaCl	NaCl	NaCl	NaCl
β_{Na+}	$\times 10^{-8} \text{ m}^2/\text{sV}$	Crow (1988)	5.20	5.20	5.20	5.20	5.20	5.20
β_{H+}	$\times 10^{-8} \text{ m}^2/\text{sV}$	Crow (1988)	36.3	36.3	36.3	36.3	36.3	36.3
β_{Cl-}	$\times 10^{-8} \text{ m}^2/\text{sV}$	Crow (1988)	7.90	7.90	7.90	7.90	7.90	7.90
β_{OH-}	$\times 10^{-8} \text{ m}^2/\text{sV}$	Crow (1988)	20.5	20.5	20.5	20.5	20.5	20.5
pK_1	(-)	Revil and Glover (1998)	7.53	7.53	7.53	7.53	7.53	7.53
pK_2	(-)	Revil and Glover (1998)	10.3	10.3	10.3	10.3	10.3	10.3
<i>Interface parameters</i>								
β_{Stem}	$\times 10^{-9} \text{ m}^2/\text{sV}$	Revil and Glover (1997)	5	5	5	5	5	5
Γ_s^0	Sites/ nm^2	Revil and Glover (1998)	10	10	10	10	10	10
pK_{me}	(-)	Kosmulski (1996)	7.5	7.5	7.5	7.5	7.5	7.5
$pK(-)$	(-)	See text for references	7.5	8.0	7.5	7.65	7.55	7.5
χ_ζ	$\times 10^{-9} \text{ m}$	Revil et al. (1999a)	2.40	2.40	2.40	2.40	2.40	2.40

Table 2 continued

Parameter	Units	Source	Berea sandstone	Boise sandstone	Detrital Fontainebleau sandstone F1D and F2D	Overgrown Fontainebleau sandstone F3Q and F4Q	Detrital Lochaline sandstone L1D and L2D	Overgrown Lochaline sandstone L3Q and L4Q
Samples			BR1, BR2 and BR3 (a)	B1II, B2II and B3I (b)	(c)	(d)	(e)	(f)
Part of Figs. 2 and 3			(a)	(b)	(c)	(d)	(e)	(f)
Σ_{prot}	$\times 10^{-8}$ S	Calculated	15.1	50	0.24	0.24	0.23	0.68
<i>Microstructural rock parameters (only used for C_{sp} modelling)</i>								
d_{gr}	$\times 10^{-4}$ m	Measured	1.657	12.9	2.33	2.53	2.655	2.775
m	(-)	Measured	1.72	1.78	1.695	1.615	1.525	1.325
F	(-)	Measured	10.44	6.42	11.13	532.74	12.74	91.83
ϕ	(-)	Measured	0.256	0.3516	0.2415	0.0205	0.1885	0.033
<i>Model variables</i>								
T	$^{\circ}\text{C}$	Measured	22.47	26	24.6	25	26.65	25.85
pH_{expt}	(-)	Measured	7.5	6.58	6.405	6.495	7.265	7.135
$pH_{\text{st.dev.}}$	(-)	Measured	± 0.72	± 0.84	± 0.35	± 0.20	± 0.175	± 0.50

'Measured' indicates an independent laboratory measurement or a parameter directly calculated from such measurements. 'Calculated' indicates that the parameter is calculated in the model (Figs. 2 and 3)

3.4 Mineral/Fluid Interface Parameters

There are six parameters which describe the mineral/fluid interface. Of these, the ionic mobility in the Stern layer β_{Stern} , the surface site density Γ_{o} , the binding constant for cation adsorption pK_{Me} , and the shear plane distance χ_{ζ} have all been held constant throughout this work (Table 1). Each, however could be adjusted within the limits imposed by the independent experimental measurements that are noted in Walker et al. (2014) and discussed fully in Glover et al. (2012). The Stern layer mobility has been taken as $\beta_{\text{Stern}} = 5 \times 10^{-9} \text{ m}^2/\text{s/V}$ from Revil and Glover (1997), the surface site density has been taken as $\Gamma_{\text{o}} = 10 \text{ sites/nm}^2$ from Revil and Glover (1998) and the binding constant for cation adsorption has been taken as $pK_{\text{Me}} = 7.5$ from Kosmulski (1996). The shear plane distance (χ_{ζ}). The model is sensitive to this parameter because it defines where in the diffuse layer the ζ is measured. In this work, it was held constant at $\chi_{\zeta} = 2.4 \times 10^{-9} \text{ m}$ for all the samples.

The fifth interface parameter is the specific surface conduction. In this paper we use it to provide a measurement of the protonic surface conduction (Σ_{prot}) for each of the rock samples. The specific surface conduction was calculated from the measured surface conductivity σ_{s} using the modal grain diameter d_{gr} , and the cementation exponent m and formation factor F for each sample. The surface conductivity was taken to be the conductivity that was measured when the rock was saturated with the lowest salinity equilibrium fluid. These surface conductivities were converted to surface conductances Σ_{s} using the relationship

$$\sigma_{\text{s}} = 2\Sigma_{\text{s}}/\Lambda, \quad (8)$$

where Λ is a characteristic length scale for the pores of the rock that was introduced by Johnson et al. (1986) and which can be calculated with the equation (Revil and Cathles 1999)

$$\Lambda = d_{\text{gr}}/2mF. \quad (9)$$

Consequently, Eqs. (8) and (9) provide individual values of surface conductance Σ_{s} for each sample. There are three contributions to surface conduction, arising from (1) the movement of protons on the surface, (2) ionic mobility in the Stern plane, and (3) ionic mobility in the diffuse layer. We have assumed that the value of surface conductance calculated using Eqs. (8) and (9) above is the same as the protonic surface conduction. This assumption has been justified by using the model to calculate and compare the three contributions to surface conduction as a function of salinity and pH. In all cases the calculated contributions to surface conduction from the diffuse layer and Stern layer were more than two orders of magnitude less than the calculated total surface conductance at all values of pH and salinity. Hence, it was possible to say that the remaining contribution, that of the protonic surface conduction, makes up the great majority of the surface conduction, and that $\Sigma_{\text{prot}} \approx \Sigma_{\text{s}}$. Consequently, for the purposes of this paper, Σ_{prot} is completely defined by independent measurements of σ_{s} , d_{gr} , m and F . The surface conductivity can also be obtained empirically from the formation factor measured at ultra-low salinities and the pore fluid conductivity, as implemented by Lorne et al. (1999a, b) and others, but this approach is more suited to experimental research rather than modelling.

The last interface parameter is the disassociation constant for dehydrogenization of silanol $pK_{(-)}$. It has been taken to vary in the restricted range $8.1 > pK_{(-)} > 7.3$, which fall in the middle of the range of values given by other researchers: $pK_{(-)} = 6.8$ (Dove and Rimstidt 1994), $pK_{(-)} = 6.5$ (Kosmulski 1996), $pK_{(-)} = 7.5$ (Hiemstra and van Riemsdijk 1990), and $pK_{(-)} = 8.5$ (Rustad et al. 1998). In this paper we have varied it only within this restrictive range in order to obtain an optimum fit of the model curves to the experimental data. It is the

only parameter which has been varied in this way since the modified model does not now contain a zeta potential offset parameter as described below.

3.5 The Zeta Potential Offset

In earlier modelling (Glover and Déry 2010; Glover et al. 2012; Glover et al. 2015) there was an additional mineral/fluid interface parameter called the zeta potential offset (ζ_0). In this work, the zeta potential offset has been replaced by a procedure which holds ζ constant at high salinities, which models the attainment of a maximum charge density in the diffuse layer as it is compressed to the thickness of one hydrated metal ion in thickness according to the hypothesis of Jaafar et al. (2009). This modelling procedure recognises the onset of such behaviour and keeps the ζ constant at salinities higher than this onset value. The values of constant ζ obtained using this approach vary with pH, as noted in the experimental measurements of Walker and Glover (2017) and produce values which are in the same range (-8 to -20 mV) as those obtained in earlier modelling (Glover and Déry 2010; Glover et al. 2012, 2015).

The previous method was essentially the addition of an ‘ad hoc’ parameter that allowed the model to work at high salinities while retaining its precision at low and medium salinities. The addition was not carried out with regard to any underlying physics and could be viewed as a parameter that could be varied to ensure a better fit of the model to the data. However, values of zeta potential offset found in this way had a very restricted range, indicating that they were the result of some unknown physical process (Glover and Déry 2010; Glover et al. 2012). The new method accepts the hypothesis of Jaafar et al. (2009) and has the advantages of (1) removing the only arbitrary parameter from the model, (2) reducing the number of variables in the model (to one in this work), and (3) having the modified model based more soundly on our understanding of the physical process occurring in the porous rocks.

3.6 Rock Microstructural Parameters

Finally, there are five parameters which describe the microstructure of the rock sample. Only three of them, however, are independent. The parameters are the modal grain size d_{gr} , porosity ϕ , cementation exponent m (Glover and Déry 2010), formation factor F , and characteristic pore size Λ . They are inter-related by Eq. (9) and Archie’s first law (e.g., Glover et al. 2015)

$$F = \phi^{-m}. \quad (10)$$

It is worth noting that it is also possible to express the theoretical model in terms of pore size d_p (Glover and Walker 2009) and pore throat size d_{pt} (Glover and Déry 2010) using the relationships

$$d_p = d_{gr} \sqrt{\frac{8\phi^{2m}}{am^2}}, \quad (11)$$

$$d_{pt} \approx d_p / 1.665, \quad (12)$$

respectively. In this work, we have opted to use grain size, porosity and cementation exponents as the three independent parameters to describe the microstructure of each rock sample.

We have obtained all of the microstructural parameters independently of the electrokinetic measurements by measuring (1) the electrical conductivity of the sample at each of the experimental salinities, (2) the electrical conductivity of each of the experimental fluids after equilibration, (3) the porosity of the sample with a range of different methods, and (iv)

the modal grain size by laser diffractometry. The microstructural parameters that were used in the modelling are shown in tables later in the paper.

3.7 Degrees of Freedom

Consequently, the model has a number of different types of parameter as summarised in Table 1. There are 3 model variables, which are parameters to which C_{sp} and ζ are known to be sensitive and which have been varied to explore these relationships, 4 fundamental physical quantities, 12 pore fluid and interface parameters which are defined by external measurements and held constant during the modelling, 5 microstructural parameters that are defined by petrophysical measurements that have been carried out on the samples and consequently also held constant during the modelling. There is only one parameter, the disassociation constant for the dehydrogenisation of silanol $pK(-)$, which has been varied to improve the fit of the model to the experimental data, and then only within the very restricted range ($8.1 > pK(-) > 7.3$) which has been fixed by independent measurements from other authors. Consequently, the degree to which the model curves presented in this work fit the experimental data is not a consequence of varying a large number of parameters until some sort of fit is attained, but the result of varying one parameter over a small range and having all the other parameters fixed by independent measurements on the particular samples or other parameters measured by independent researchers.

4 Theoretical Modelling Results

Since we know the microstructural (porosity, cementation exponent and modal grain size) and the experimental fluid parameters (equilibrated salinity, electrical conductivity and pH) for each sample, we have been able to carry out modelling of individual samples as well as for aggregated lithofacies.

In this section the figures and discussion of the ζ modelling are followed by those related to the C_{sp} , which is the order in which they are calculated in the theoretical model. Despite this order, it should be remembered that for the experimental results, it is the C_{sp} that is derived first, directly from streaming potential and pressure difference measurements, while the ζ is derived subsequently from the C_{sp} using additional parameters.

4.1 Modelling by Lithofacies

Figures 2 and 3 show, respectively, all of the ζ and C_{sp} modelling curves we have calculated for each of the six lithofacies (Berea, Boise, and detrital and overgrowth forms of both Fontainebleau and Lochaline sandstones) from this paper compared with all of the data for these lithofacies from Walker and Glover (2017). The modelled curves extend for the complete relevant salinity range (10^{-5} – 10 mol/dm³) and from pH 6 to pH 8 in increments of half a pH unit. In each case the curves are calculated for the temperature at which the experimental measurements were taken. The lithofacies modelling was carried out with mean values of the microstructural parameters for each lithofacies and which are shown in Table 2.

Figure 2 shows the calculated ζ model curves as a function of salinity and pH together with the data from Walker and Glover (2017) and arranged by lithofacies. The model curves use mean microstructural parameters for the samples composing each lithofacies.

A number of conclusions may be drawn from comparison of the modelled curves with the experimental data. First, that the quality of the experimental data is better than was previously

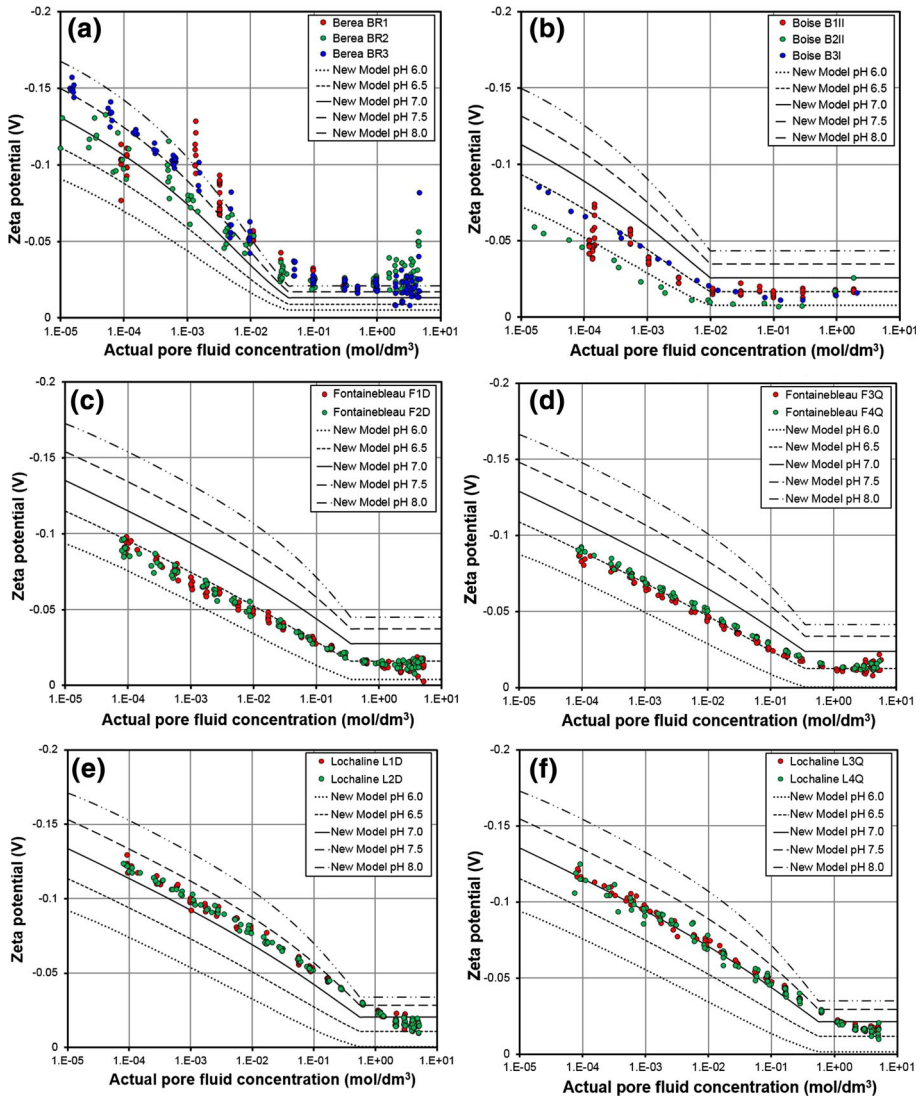


Fig. 2 Modelled ζ (curves) for all facies types as a function of pore fluid salinity and pH , compared with the experimental measurements of ζ (symbols) from this paper. **a** Berea sandstone, **b** Boise sandstone, **c** detrital Fontainebleau sandstone, **d** overgrown Fontainebleau sandstone, **e** detrital Lochaline sandstone, and **f** overgrown Lochaline sandstone. All model parameters are shown in Table 2. The ζ part of the model has 16 independent parameters, of which 3 are model variables (temperature, fluid salinity and pH), and 13 are predefined by the electro-chemistry of the fluid and fluid–mineral interface. ζ does not depend on the microstructure of the rock in this implementation of the theoretical model. The model retains only 1 variable parameter ($pK_{(-)}$), which was allowed to vary in the experimentally restricted range $8.0 > pK_{(-)} > 7.5$

available [collated in Glover et al. (2012)], both in its smaller uncertainty (scatter) and because the temperature, salinity and pH of the equilibrated pore fluids have been measured reliably and reported together with the C_{sp} and ζ data. This enables the modelling values for a particular temperature, pore fluid salinity and pH to be compared directly with their measured values.

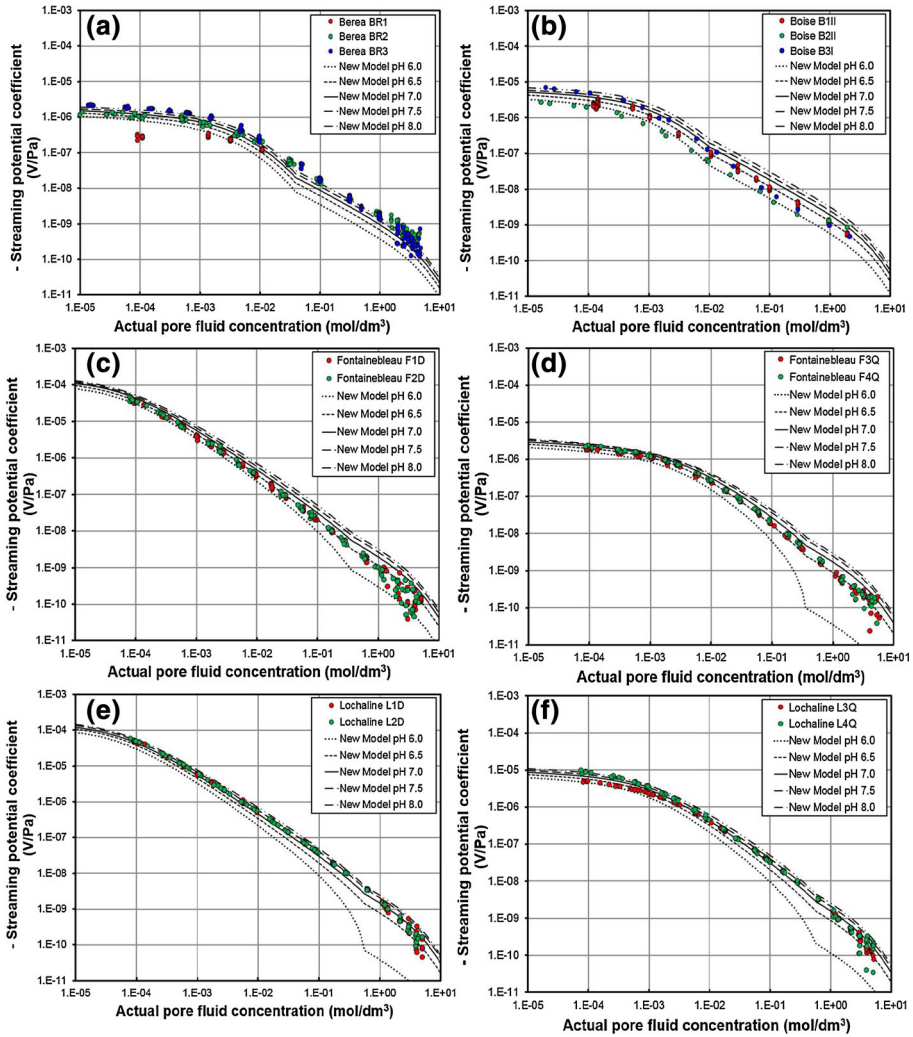


Fig. 3 Modelled C_{sp} (curves) for all facies types as a function of pore fluid salinity and pH , compared with the experimental measurements of C_{sp} (symbols) from this paper. **a** Berea sandstone, **b** Boise sandstone, **c** detrital Fontainebleau sandstone, **d** overgrown Fontainebleau sandstone, **e** detrital Lochaline sandstone, and **f** overgrown Lochaline sandstone. All model parameters are shown in Table 2. In this model, there are 19 independent parameters, of which 3 are model variables (temperature, fluid salinity and pH), 13 are predefined by the electro-chemistry of the fluid and fluid-mineral interface, and 3 are predefined by the rock microstructure (d_{gr} , m , ϕ). The model retains only 1 variable parameter ($pK(-)$), which was allowed to vary in the experimentally restricted range $8.0 > pK(-) > 7.5$

Second, the modelled ζ curves reproduce all of the main features of the ζ data, with magnitude of the ζ increasing as the logarithm of the salinity as pore fluid salinity is reduced. The ζ model curves are also extremely sensitive to pore fluid pH , as was noted when Walker and Glover (2017) discussed the experimental dataset. This is shown by the spread of the model curves as a function of pH and the degree to which the experimentally measured ζ data concord with the modelled ζ curve for the experimentally determined value of pH , for each sample. There is a greater degree of scattering of the experimental data at high salinities, where

measurements are difficult to make (Vinogradov et al. 2010; Walker et al. 2014; Walker and Glover 2017). However, the model ζ curves agree well with the mean of this cloud of points.

Figure 3 shows the calculated C_{sp} model curves as a function of pore fluid salinity and pH together with the data from Walker and Glover (2017) and arranged by lithofacies.

Once again, it is clear that the C_{sp} model curves reproduce all of the main features of the experimentally measured data, with the value of C_{sp} increasing in an approximately power law fashion as pore fluid salinity is reduced. The C_{sp} model curves are also sensitive to pore fluid pH , but not to the same degree as the ζ curves, and this is also noted in the experimental data.

It was hypothesised by Glover et al. (2012) that the flattening of C_{sp} at low salinities, which is clear in experimental data (e.g., Walker and Glover 2017) is controlled by the development of surface conduction and the microstructure of the rocks on the basis of a comparison of their model with the experimental data then available. Comparison of the modelling carried out in this paper with the new data in Walker and Glover (2017) has confirmed the effect. Our C_{sp} modelling for each of the two microstructural forms of Lochaline and Fontainebleau sandstone (i.e., between parts (c) and (d) and parts (e) and (f) in Fig. 3) shows that variations in their independently measured microstructural parameters (modal grain size, porosity, cementation exponent and/or formation factor) and surface conduction (in the absence of any mineralogical differences) are sufficient to explain the degree of flattening occurring in the experimental C_{sp} data. In each case the quartz overgrown version shows a greater degree of low salinity flattening, and this is well-modelled by smaller porosities and cementation exponents which occur for these samples (the measured grain sizes and values of surface conduction are not significantly different).

It should be noted that there is no microstructural control on zeta potential because it is a property of the electrical double layer (EDL) which occurs between the mineral grain and the pore fluid and can be regarded as a property acting on a grain surface scale, independent of how those grains are arranged in a microstructure. This is discussed in more detail at the end of Sect. 4.2.

4.2 Sample-by-Sample Modelling

The model has been implemented for each sample measured by Walker and Glover (2017) for a range of salinities and pH at the experimental temperature and with the microstructural and electrical parameters (modal grain size, porosity, cementation exponent, and formation factor) that were measured for that sample.

As in the case of the modelling by lithofacies, the electro-chemical parameters that describe the interface between the rock matrix and the pore fluid could be adjusted to ensure a best fit. However, once again, only one was varied ($pK_{(-)}$). The full sample parameters and the modelling parameters are shown in Table 3. Figures 4 and 5 show the sample-specific ζ and C_{sp} curves from the theoretical model as well as the relevant experimental data from that sample, for C_f ranging from 10^{-5} to 10 mol/dm³ and for five values of pH in the range $6 < pH < 8$. The pH of the pore fluid was controlled and measured during the experiments of Walker and Glover (2017) to within ± 0.2 , which is given as pH_{expt} in the data tables in this paper. This value should be used to interpret how the values of the experimental data in Figs. 4 and 5 compare with the set of modelled ζ and C_{sp} curves for the five values of pH for which modelling has been implemented.

Overall, both theoretical ζ and C_{sp} model curves agree extremely well with the experimental data for individual samples; better than when calculated for the generic lithofacies. This implies that modelling ζ and C_{sp} benefits from knowledge of individual sample properties. Accord between the experimental data and the modelling was particularly good for

Table 3 The parameters used in the modelling of the C_{sp} and ζ for individual samples (Figs. 4 and 5)

Parameter	Units	Source	Berea sandstone			Boise sandstone			Fontainebleau sandstone				Lochaline sandstone			
			BR1	BR2	BR3	B1II	B2II	B3I	F1D	F2D	F3Q	F4Q	L1D	L2D	L3Q	L4Q
<i>Fluid parameters</i>																
<i>Fluid type</i>																
β_{Na+}	$\times 10^{-8} \text{ m}^2/\text{sV}$	Crow (1988)	NaCl	NaCl	NaCl	NaCl	NaCl	NaCl	NaCl	NaCl	NaCl	NaCl	NaCl	NaCl	NaCl	NaCl
β_{H+}	$\times 10^{-8} \text{ m}^2/\text{sV}$	Crow (1988)	5.20	5.20	5.20	5.20	5.20	5.20	5.20	5.20	5.20	5.20	5.20	5.20	5.20	5.20
β_{Cl-}	$\times 10^{-8} \text{ m}^2/\text{sV}$	Crow (1988)	36.3	36.3	36.3	36.3	36.3	36.3	36.3	36.3	36.3	36.3	36.3	36.3	36.3	36.3
β_{OH-}	$\times 10^{-8} \text{ m}^2/\text{sV}$	Crow (1988)	7.90	7.90	7.90	7.90	7.90	7.90	7.90	7.90	7.90	7.90	7.90	7.90	7.90	7.90
pK_1	(-)	Revil and Glover (1998)	20.5	20.5	20.5	20.5	20.5	20.5	20.5	20.5	20.5	20.5	20.5	20.5	20.5	20.5
pK_2	(-)	Revil and Glover (1998)	7.53	7.53	7.53	7.53	7.53	7.53	7.53	7.53	7.53	7.53	7.53	7.53	7.53	7.53
<i>Interface parameters</i>																
β_{Stem}	$\times 10^{-9} \text{ m}^2/\text{sV}$	Revil and Glover (1997)	10.3	10.3	10.3	10.3	10.3	10.3	10.3	10.3	10.3	10.3	10.3	10.3	10.3	10.3
Γ_s^0	Sites/nm ²	Revil and Glover (1998)	5.00	5.00	5.00	5.00	5.00	5.00	5.00	5.00	5.00	5.00	5.00	5.00	5.00	5.00
pK_{me}	(-)	Kosmulski (1996)	10	10	10	10	10	10	10	10	10	10	10	10	10	10
$pK_{(-)}$	(-)	See text for references	7.5	7.5	7.5	7.5	7.5	7.5	7.5	7.5	7.5	7.5	7.5	7.5	7.5	7.5
χ_ζ	$\times 10^{-9} \text{ m}$	Revil et al. (1999a)	7.5	7.5	7.5	7.5	7.5	7.5	7.5	7.5	7.5	7.5	7.5	7.5	7.5	7.5
			2.40	2.40	2.40	2.40	2.40	2.40	2.40	2.40	2.40	2.40	2.40	2.40	2.40	2.40

Table 3 continued

Parameter	Units	Source	Berea sandstone			Boise sandstone			Fontainebleau sandstone				Lochaline sandstone			
			BR1	BR2	BR3	B1III	B2II	B3I	F1D	F2D	F3Q	F4Q	L1D	L2D	L3Q	L4Q
Part of Figs. 4 & 5			(a)	(b)	(c)	(d)	(e)	(f)	(g)	(h)	(i)	(j)	(k)	(l)	(m)	(n)
Σ_{prot}	$\times 10^{-8}$ S	Measured	50.1	15.1	15.1	49.6	50.1	40.1	0.29	0.3	0.25	0.25	0.262	0.252	0.601	0.68
<i>Microstructural rock parameters (only used for C_{sp} modelling)</i>																
d	$\times 10^{-4}$ m	Measured	1.8	1.55	1.62	7.39	9.91	21.4	2.35	2.31	2.51	2.55	2.63	2.68	2.77	2.78
m	(-)	Measured	1.79	1.72	1.66	1.569	1.677	1.811	1.71	1.68	1.60	1.63	1.50	1.55	1.33	1.32
F	(-)	Measured	10.22	10.63	10.47	6.53	5.65	7.48	11.64	10.62	567.54	503.33	13.09	12.4	142.67	65.66
ϕ	(-)	Measured	0.272	0.253	0.243	0.3024	0.3561	0.3292	0.238	0.245	0.019	0.022	0.180	0.197	0.024	0.042
<i>Model variables</i>																
T	$^{\circ}\text{C}$	Measured	25.8	20.1	21.5	26	26	26	24.5	24.7	25.1	24.9	27.2	26.1	25.9	25.8
pH_{expt}	(-)	Measured	8.03	7.05	7.41	7.2	5.94	6.61	6.40	6.41	6.48	6.51	7.27	7.26	7.15	7.12
$pH_{\text{st.dev.}}$	(-)	Measured	± 0.41	± 0.21	± 0.11	± 0.54	± 0.24	± 0.086	± 0.15	± 0.20	± 0.10	± 0.10	± 0.20	± 0.15	± 0.20	± 0.30

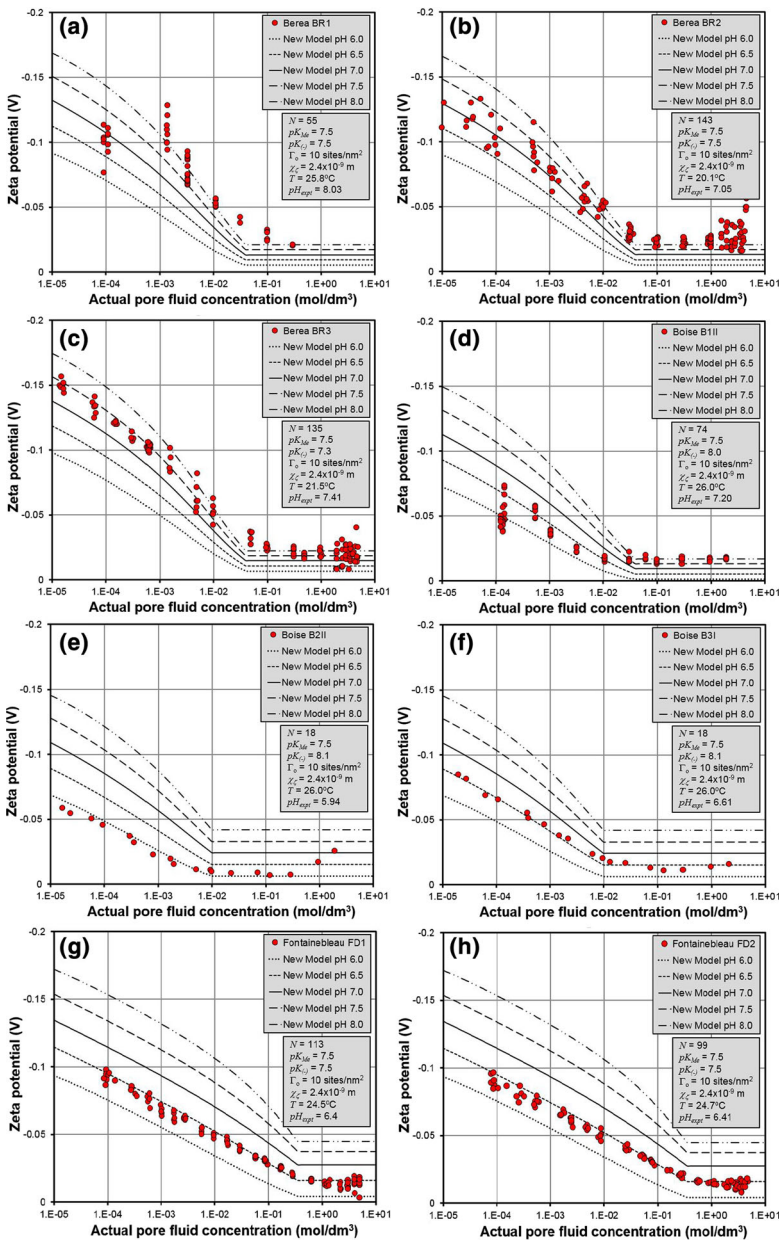


Fig. 4 Modelled ζ (curves) for individual samples as a function of pore fluid salinity and pH , compared with the experimental measurements of ζ (symbols) from this paper. **a** Berea (BR1), **b** Berea (BR2), **c** Berea (BR3), **d** Boise (B1II), **e** Boise (B2II), **f** Boise (B3I) **g** Fontainebleau (F1D), **h** Fontainebleau (F2D), **i** Fontainebleau (F3Q), **j** Fontainebleau (F4Q), **k** Lochaline (L1D), **l** Lochaline (L2D), **m** Lochaline (L3Q), and **n** Lochaline (L4Q). All model parameters are shown in Table 3. In this model, there are 16 independent parameters, of which 3 are model variables (temperature, fluid salinity and pH), and 13 are predefined by the electro-chemistry of the fluid and fluid-mineral interface. ζ does not depend on the microstructure of the rock in this implementation of the theoretical model. The model retains only 1 variable parameter ($pK(-)$), which was allowed to vary in the experimentally restricted range $8.1 > pK(-) > 7.3$. Please note that there are multiple experiments at the same salinity carried out for sample BR1 as this sample was used to develop the experimental protocol

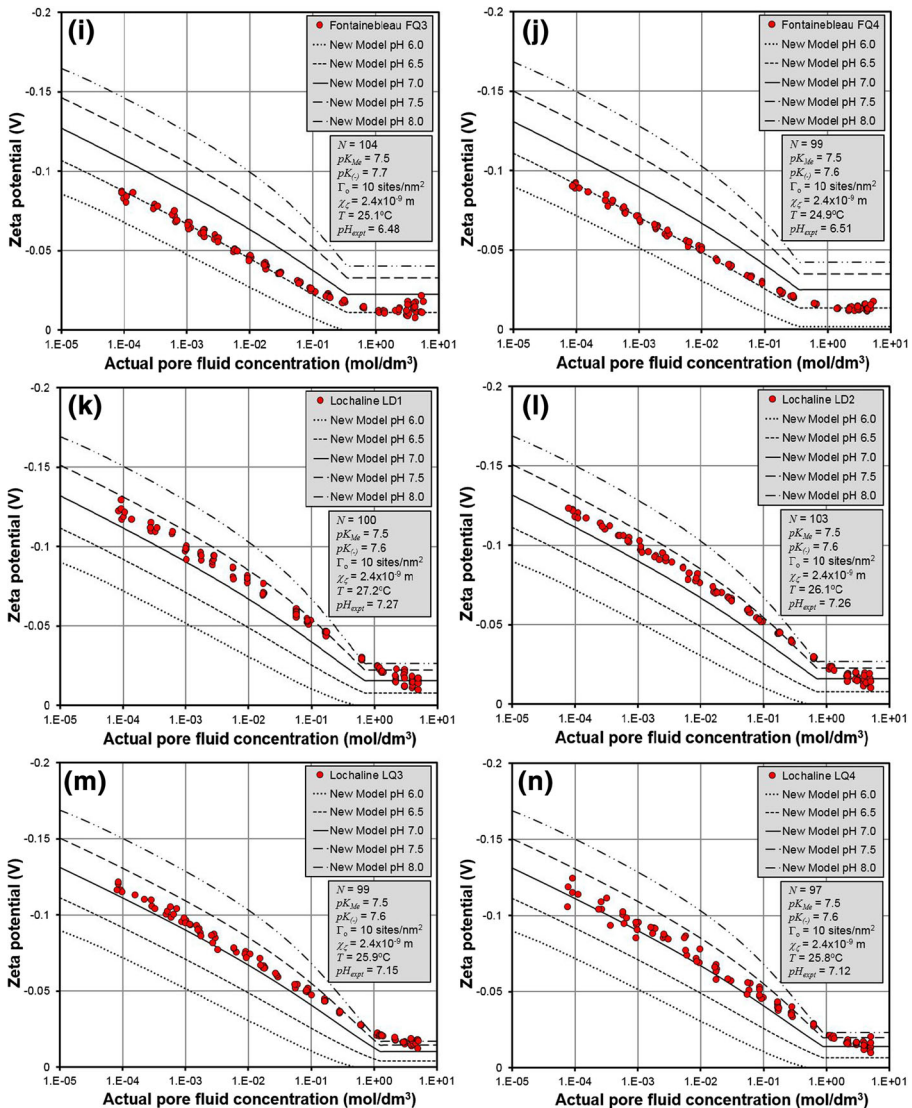


Fig. 4 continued

the Fontainebleau and Lochaline sandstone samples. For example, the data for the sample of detrital Fontainebleau sandstones F1D and F2D, shown in Fig. 4g, h, fall clearly on the curve for a $pH=6.5$ in each diagram. The experimentally measured pH for these measurements was $pH_{exp} = 6.40$ and 6.41 . The data for the Berea and Boise sandstones have a greater scatter, however, even here the mean behaviour agrees very well with the theoretical curves. For example, the Berea sandstone sample BR3 has ζ and C_{sp} data that follow a trend the mean behaviour of which would lie on a theoretical curve for $pH 7.5$, while the measured pH during the experiment was $pH_{exp} = 7.41$.

Considering the ζ modelling, Fig. 4 shows the calculated curves modelled for individual samples. It is clear that the ζ model curves reproduce the overall low to medium salinity logarithmic behaviour of the experimental data well. The high salinity behaviour of the

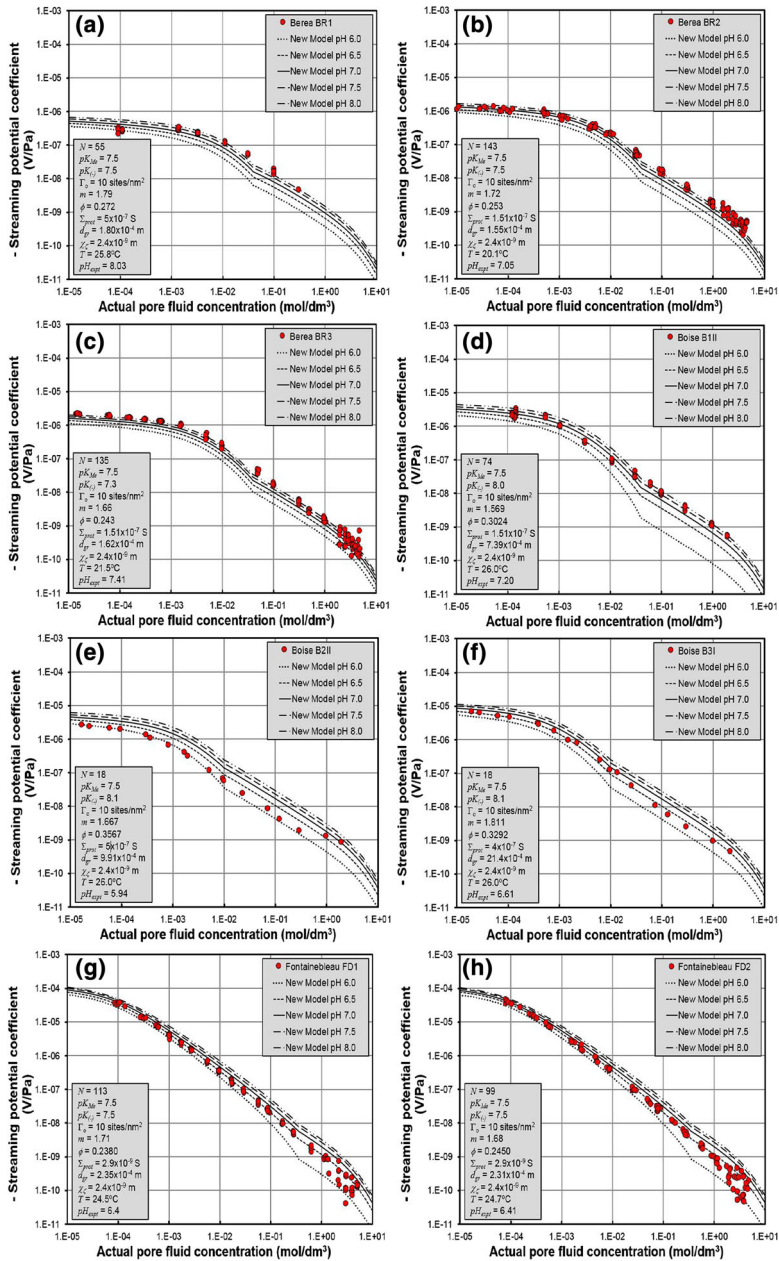


Fig. 5 Modelled C_{sp} (curves) as a function of pore fluid salinity and pH , compared with the experimental measurements of C_{sp} (symbols). **a** Berea (BR1), **b** Berea (BR2), **c** Berea (BR3), **d** Boise (B11), **e** Boise (B21), **f** Boise (B31) **g** Fontainebleau (F1D), **h** Fontainebleau (F2D), **i** Fontainebleau (F3Q), **j** Fontainebleau (F4Q), **k** Lochaline (L1D), **l** Lochaline (L2D), **m** Lochaline (L3Q), and **n** Lochaline (L4Q). All model parameters are shown in Table 3. In this model, there are 19 independent parameters, of which 3 are model variables (temperature, fluid salinity and pH), 13 are predefined by the electro-chemistry of the fluid and fluid-mineral interface, and 3 are predefined by the rock microstructure (d_{gr} , m , ϕ). The model retains only 1 variable parameter ($pK(-)$), which was allowed to vary in the experimentally restricted range $8.1 > pK(-) > 7.3$. Apparently incomplete curves represent negative values that cannot be plotted on a logarithmic axis

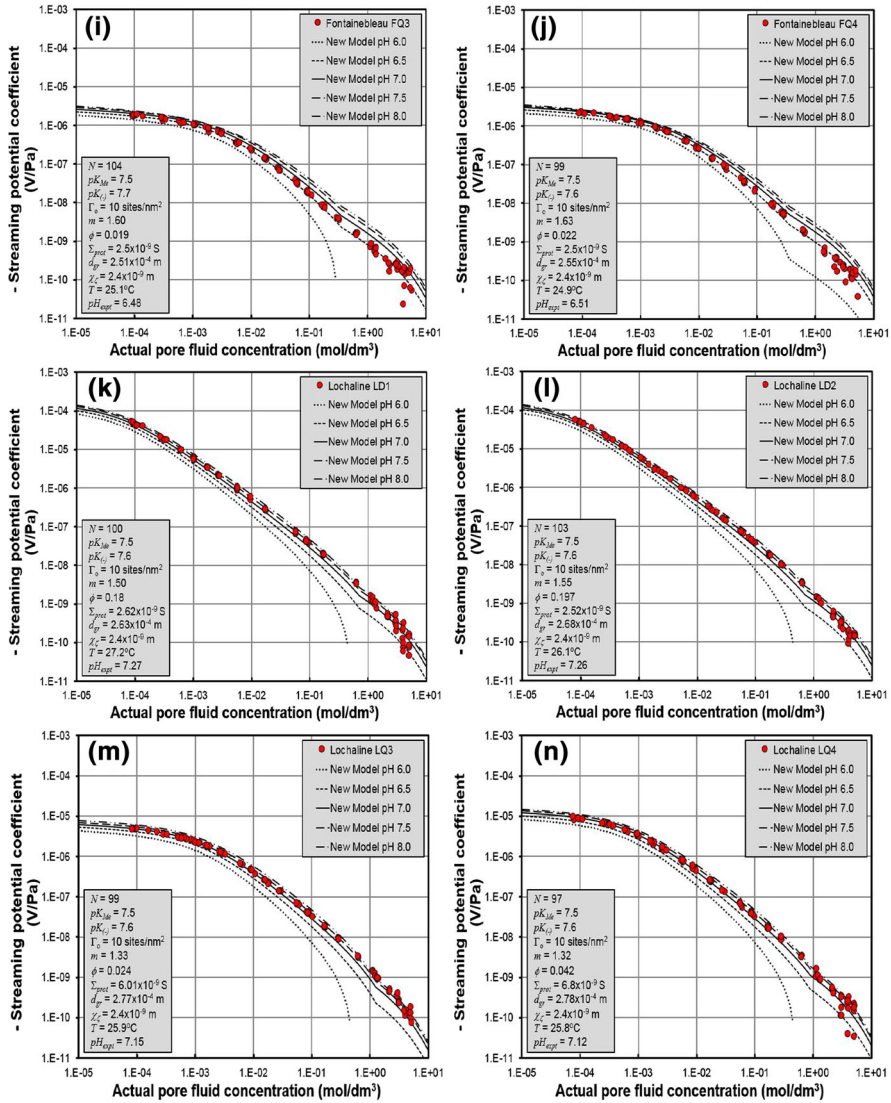


Fig. 5 continued

experimental data is also modelled well by replacing the ad hoc ζ offset that was used in previous models with our new approach, which keeps the ζ at a constant level for salinities above which the thickness of the diffuse layer is approximately the same or less than the diameter of a hydrated metal ion.

It is clear from the experimental data that the ζ is highly sensitive to pore fluid pH . The results of modelling reproduce this pH -dependence well with the mean of the experimental data falling close to the theoretical curves for the appropriate experimental pH in all cases. For example, the mean pH of the Fontainebleau and Lochaline samples is 6.45 and 7.2, respectively. For the four samples of Fontainebleau sandstone, Fig. 4g–j shows clearly that the experimentally determined ζ fall just below the modelled curve for pH 6.5 theoretical

line, while for Lochaline sandstones, Fig. 4k–n shows the experimentally determined ζ fall between the modelled curves for pH 7 and pH 7.5.

We have calculated coefficients of determination for the comparison of the ζ data for each sample and the theoretical curve calculated for the pH at which the measurements were made (pH_{expt}) and find that the coefficient of determination (R^2) values are in all cases > 0.89 . Hence the experimental observation that pH is one of the major controls on the ζ , and that even small changes in pH (e.g., pH 7 ± 1) can lead to a large change in ζ (Walker and Glover, 2017) is now supported by modelling.

Considering the C_{sp} modelling, Fig. 5 shows the modelled C_{sp} curves as a function of salinity and pH for individual samples, taking into account their individual petrophysical properties. The C_{sp} model curves reproduce all of the main features of the C_{sp} data extremely well. The overall approximate power law behaviour is overlain with a flattening at low salinities and curvature at moderate salinities for some values of pH , both of which conform to the experimental data. In general, the use of sample-specific parameters improves the agreement between the theoretical model curves and the experimental data compared to the modelling in Fig. 3, and the agreement between the theory and the experimental data is in many cases excellent.

Disagreement occurs for specific salinities where there may be systematic errors in the experimental data (e.g., for 10^{-4} mol/dm³ for Berea sandstone BR1, Fig. 5a), and there is an overestimation of the theoretical model at low salinities for the Boise sandstone samples (i.e., for B1II, B2II and B3I, Fig. 5d–f), which probably arises from using inappropriate modelling parameters. The agreement could be improved if we had taken the approach of fitting the theoretical model to the experimental data, but the goal of this work was not to fit the theoretical model to the data but to see how robust the theoretical model is when compared to high-quality data. The agreements between theory and experiment in the sample-by-sample study represented by Figs. 3 and 5 are better than any published so far.

The C_{sp} model curves are sensitive to pore fluid pH just as in Fig. 3, but now it is possible to see clearly that the experimental data fall close to the theoretical curve for the experimental value of pH (pH_{expt}), which is given for reference on each plot and in Table 3, together with the uncertainty in its measurement. A typical example is for Berea sample BR3 (Fig. 5c), where the experimental data fall almost exactly on the curve for pH 7.5 and for which the mean experimental pH was 7.41 ± 0.11 (Table 3). We have calculated coefficients of determination for the comparison of the C_{sp} data for each sample and the theoretical curve calculated for the pH at which the measurements were made (pH_{expt}), and find that the R^2 values are in all cases > 0.91 .

The microstructural control of the flattening of the C_{sp} model curves at low salinities is completely clear in the sample-by-sample modelling. Comparison between the detrital Fontainebleau sandstones (F1D and F2D, Fig. 5g, h) with the overgrown Fontainebleau sandstones (F3Q and F4Q, Fig. 5i, j), and similarly for the detrital and overgrown forms of Lochaline sandstone (L1D and L2D, Fig. 5k, l with L3Q and L4Q, Fig. 5m, n) shows that there is a much stronger degree of flattening at low salinities for the authigenic overgrown forms of the sandstone than the detrital sandstones. The implementation of these microstructural parameters in each theoretical curve allows the curves to match the experimental data and take into account the effect of the microstructural differences on the measured C_{sp} data. The microstructural differences between the detrital and authigenic overgrown sandstones is marked, with the overgrown samples of either rock type having (1) a much smaller porosity, (2) a much larger formation factor, (3) a slightly larger grain size, and (4) a similar or slightly smaller cementation exponent. These changes indicate that, from an electrical point of view, the development of overgrowths fills most of the pores without reducing the degree to which

the pores are connected, leaving the cementation exponent relatively unchanged. After the overgrowths are developed, electrically patent pathways still occur along thin passageways between the euhedral grains, but their sensitivity to closure, which is measured by the large formation factor, is high. The increase in formation factor is primarily due to the significant reduction in porosity than a change in cementation exponent. There is little change in grain size because the overgrowths are filling-in pore space rather than increasing the size of the grain in all directions. This is akin to comparing the diameter of a sphere with a co-centred cube of the same linear dimensions—the cube has a volume that is almost twice as big ($6/\pi = 1.9099$), yet seems to occupy a similar amount of space.

Once again, it should be noted that there is no microstructural control on zeta potential. The zeta potential is a property of the electrical double layer (EDL) which occurs between the mineral grain and the pore fluid. It is calculated from the Stern potential which itself is obtained by assuming that the EDL is thin compared to its extent (Fixman 1980, 1983). Consequently, it can be regarded as a property acting on a grain surface scale and should be independent of how those grains are arranged in a microstructure. That will certainly be the case when the EDL is extremely small at high pore fluid salinities. However, there is a possibility that the zeta potential might vary in a rock at a local scale when the pore fluid salinity is so low that the EDL is of the same scale as the characteristic scale of the pores. In this case, the shear plane might vary from location to location within the microstructure as fluid flow conforms to that microstructure. This will give rise to local, transient potential differences which can be regarded as microstreaming potentials. However, the electro-neutrality requirement will ensure that most of these microstreaming potentials cancel each other out so that we are left with the macroscopic overall streaming potential. A similar effect can also be imagined to arise from a rock composed of a mixture of minerals with different Stern potentials and consequently different zeta potentials. Consequently, the effect will have an influence on how the zeta potential from two different minerals in a two-mineral mixture mix to provide an effective zeta potential.

5 Conclusions

A modified form of the theoretical model of Glover et al. (2012) has been applied to all of the data from Walker and Glover (2017) for each lithofacies and for each individual sample. The major modifications to the model comprised (1) implementing a calculation for pore fluid pH that is a function of all the ionic contributions to the electrolyte, (2) removing the zeta potential offset as a parameter forcing a constant ζ at high salinities, (3) implementing a variable threshold ζ at high salinities where the thickness of the diffuse layer is comparable to the size of the hydrated metal ions and representing, therefore, a maximum charge density for the diffuse layer. The modelling was carried out as a function of salinity and pH allowing only one parameter (the disassociation constant for dehydrogenation of silanol) to vary over a small range constrained by independent measurements made by other researchers.

The modelled ζ curves were found to agree well with the experimental data for each lithofacies and extremely well for each individual sample. The modelled ζ is highly sensitive to pH and salinity, and it was found that the experimental data fell on the curves expected from the experimental pH, in most cases to within ± 0.2 pH points, contrasting with the widespread scatter of previously existing ζ measurements which suffered a lack of pH control.

The modelled C_{sp} curves were also found to agree well with the experimental data for each lithofacies and extremely well for each individual sample. It has been confirmed that

the low salinity behaviour of the C_{sp} measurements is caused by the pore structure and best exemplified by the difference results obtained when measuring either the detrital or overgrown forms of the Fontainebleau and Lochaline data, each of which is chemically indistinguishable.

The replacement of the zeta potential offset with an implementation of the maximum charge density hypothesis of Vinogradov et al. (2010) for generating a constant value of ζ at high salinities (to match the experimental observations) has led to a modelling which concords extremely well with all of the data in the Walker and Glover (2017) dataset.

It should be noted that this paper concerns itself only with sandstones. The model it describes does not take into the account the complex mineralogy of rocks that comprise clays, which affect the mineral–electrolyte interfacial chemistry. In order to make the model applicable to a wider range of rocks, a proper surface complexation model (e.g., Datta et al., 2009; Li et al., 2016) should be incorporated in order to yield the equilibrium zeta potential of each type of mineral before calculating the effective zeta potential value for each rock sample and then calculating the streaming potential from the individual rock sample microstructural parameters. The surface complexation models, when validated against experimental data, could provide a route for evaluating the zeta potential under varying concentration, composition and temperature.

Acknowledgements The funding for this work was provided by the Natural Sciences and Engineering Research Council of Canada (NSERC) Discovery Grant Programme and a start-up grant from the University of Leeds. I am indebted to two anonymous reviewers who substantially contributed to the quality of this paper.

Open Access This article is distributed under the terms of the Creative Commons Attribution 4.0 International License (<http://creativecommons.org/licenses/by/4.0/>), which permits unrestricted use, distribution, and reproduction in any medium, provided you give appropriate credit to the original author(s) and the source, provide a link to the Creative Commons license, and indicate if changes were made.

References

- Bolève, A., Crespy, A., Revil, A., Janod, F., Mattiuzzo, J.L.: Streaming potentials of granular media: influence of the Dukhin and Reynolds numbers. *J. Geophys. Res.* **112**, B08204 (2007). <https://doi.org/10.1029/2006JB004673>
- Crow, D.R.: Principles and Applications of Electrochemistry. Chapman and Hall, London (1988)
- Datta, S., Conlisk, A.T., Li, H.F., Yoda, M.: Effect of divalent ions on electroosmotic flow in microchannels. *Mech. Res. Commun.* **36**(1), 65–74 (2009)
- Dove, P.M., Rimstidt, J.D.: Silica–water interactions. *Rev. Mineral. Geochem.* **29**, 259–308 (1994)
- Fixman, M.: Charged macromolecules in external fields. I. The sphere. *J. Chem. Phys.* **72**(9), 5177–5186 (1980)
- Fixman, M.: Thin double layer approximation for electrophoresis and dielectric response. *J. Chem. Phys.* **78**(3), 1483–1491 (1983)
- Glover, P.W.J.: Electrical Properties, 2nd ed. Treatise Geophys, vol. 189. Elsevier, London (2015)
- Glover, P.W.J., Déry, N.: Dependence of streaming potential on grain diameter and pore radius for quartz glass beads. *Geophysics* **75**(6), F225–F241 (2010). <https://doi.org/10.1190/1.3509465>
- Glover, P.W.J., Walker, E.: A grain size to effective pore size transformation derived from an electro-kinetic theory. *Geophysics* **74**(1), E17–E29 (2009)
- Glover, P.W.J., Walker, E., Jackson, M.D.: Streaming-potential coefficient of reservoir rock, a theoretical model. *Geophysics* **77**(2), D17–D43 (2012). <https://doi.org/10.1190/GEO2011-0364.1>
- Hiemstra, T., Van Riemsdijk, W.H.: Multiple activated complex dissolution of metal (hydr)oxide: a thermodynamic approach applied to quartz. *J. Colloid Interface Sci.* **136**, 132–150 (1990). [https://doi.org/10.1016/0021-9797\(90\)90084-2](https://doi.org/10.1016/0021-9797(90)90084-2)
- Jaafar, M.Z., Vinogradov, J., Jackson, M.D.: Measurement of streaming potential coupling coefficient in sandstones saturated with high salinity NaCl brine. *Geophys. Res. Lett.* **36**, L21306 (2009). <https://doi.org/10.1029/2009GL040549>

- Johnson, D.L., Koplik, J., Schwartz, L.M.: New pore-size parameter characterizing transport in porous media. *Phys. Rev. Lett.* **57**(20), 2564–2567 (1986). <https://doi.org/10.1103/PhysRevLett.57.2564>
- Kosmulski, M.: Adsorption of cadmium on alumina and silica: analysis of the values of stability constants of surface complexes calculated for different parameters of triple layer model. *Colloids Surf. A* **117**, 201–214 (1996). [https://doi.org/10.1016/0927-7757\(96\)03706-5](https://doi.org/10.1016/0927-7757(96)03706-5)
- Li, S., Leroy, P., Heberling, F., Devau, N., Jougnot, D., Chiaberge, C.: Influence of surface conductivity on the apparent zeta potential of calcite. *J. Colloid Interface Sci.* **468**, 262–275 (2016)
- Lide, D.R.: *Handbook of Chemistry and Physics*, 98th edn. Taylor Francis, London (2017). ISBN 1439880492
- Phillips, S.L., Ozbek, H., Otto, R.J.: Basic energy properties of electrolytic solutions database: sixth International CODATA Conference Santa Flavia (Palermo), Sicily, Italy, May 22–25, accessed 10 June 2010. <https://www.osti.gov/bridge/purl.cover.jsp;jsessionid=3954E775156A8BC0FA35DB5CE5B402D4? purl=/6269880-iPJPhB/> (1978)
- Lorne, B., Perrier, F., Avouac, J.: Streaming potential measurements: 1. Properties of the electrical double layer from crushed rock samples. *J. Geophys. Res: Solid Earth* **104**(B8), 17857–17877 (1999a)
- Lorne, B., Perrier, F., Avouac, J.: Streaming potential measurements: 2. Relationship between electrical and hydraulic flow patterns from rock samples during deformation. *J. Geophys. Res.: Solid Earth* **104**(B8), 17879–17896 (1999b)
- Pride, S.: Governing equations for the coupled electromagnetics and acoustics of porous media. *Phys. Rev. B* **50**(21), 15678–15696 (1994)
- Pride, S.R., Morgan, F.D.: Electrokinetic dissipation induced by seismic waves. *Geophysics* **56**, 914–925 (1991). <https://doi.org/10.1190/1.1443125>
- Revil, A., Cathles, L.M.: Permeability of shaly sands. *Water Resour. Res.* **35**, 651–662 (1999)
- Revil, A., Glover, P.W.J.: Theory of ionic surface electrical conduction in porous media. *Phys. Rev. B* **55**, 1757–1773 (1997). <https://doi.org/10.1103/PhysRevB.55.1757>
- Revil, A., Glover, P.W.J.: Nature of surface electrical conductivity in natural sands, sandstones, and clays. *Geophys. Res. Lett.* **25**, 691–694 (1998). <https://doi.org/10.1029/98GL00296>
- Revil, A., Pezard, P.A., Glover, P.W.J.: Streaming potential in porous media. I. Theory of the zeta-potential. *J. Geophys. Res.* **104**(B9), 20021–20031 (1999a). <https://doi.org/10.1029/1999JB900089>
- Revil, A., Schwaeger, H., Cathless, L.M., Manhardt, P.D.: Streaming potential in porous media 2. Theory and application to geothermal systems. *J. Geophys. Res.* **104**, 20033–20048 (1999b). <https://doi.org/10.1029/1999JB900090>
- Rustad, J.R., Wasserman, E., Felmy, A.R., Wilke, C.: Molecular dynamics study of proton binding to silica surfaces. *J. Colloid Interface Sci.* **198**, 119–129 (1998). <https://doi.org/10.1006/jcis.1997.5195>
- Sen, P., Goode, P.: Influence of temperature on electrical conductivity on shaly sands. *Geophysics* **57**, 89–96 (1992a)
- Sen, P., Goode, P.: Errata, to: influence of temperature on electrical conductivity of shaly sands. *Geophysics* **57**, 1658 (1992b)
- Vinogradov, J., Jaafar, M.Z., Jackson, M.D.: Measurement of streaming potential coupling coefficient in sandstones saturated with natural and artificial brines at high salinity. *J. Geophys. Res.* **115**, B12204 (2010). <https://doi.org/10.1029/2010JB007593>
- Walker, E., Glover, P.W.J.: A transient method for measuring the DC streaming potential coefficient of porous and fractured rocks. *Transp. Porous Media* (2017). <https://doi.org/10.1002/2013JB010579>
- Walker, E., Glover, P.W.J., Ruel, J.: A transient method for measuring the DC streaming potential coefficient of porous and fractured rocks. *J. Geophys. Res.* (2014). <https://doi.org/10.1002/2013JB010579>
- Wu, L., Forsling, W., Schlindler, P.W.: Surface complexation of calcium minerals in aqueous solution. *J. Colloid Interface Sci.* **147**, 178–185 (1991). [https://doi.org/10.1016/0021-9797\(91\)90145-X](https://doi.org/10.1016/0021-9797(91)90145-X)